Finite Element Analysis and Experimental Characterisation of a Localised Steerable Tip for Soft Everting Robots

Yi Lu, Korn Borvorntanajanya, Jialei Shi, Ferdinando Rodriguez y Baena

***Abstract*— Soft everting robots, also known as vine robots, can achieve growth by everting materials at the robots' tip. As such, they offer unique advantages in navigating constrained and tortuous environments. However, understanding and modelling their steering behaviour presents significant challenges. This study combines finite element analysis with experimental characterisation to investigate the steering performance of a soft everting robot equipped with a pneumatically steerable tip, focusing on exploring key design parameters. Specifically, finite element simulations evaluate the robot's steering angles by examining the influence of manipulator dimensions and types of silicone used. Complementary experimental characterisation further assesses steering performances focusing on everting material's mechanical properties, including the effects of material thickness and stretchability. The results provide critical insights for optimising the design of pneumatically actuated tip steering mechanisms in soft everting robots, with particular relevance to medical applications where proper material selection and dimensional optimisation are essential.**

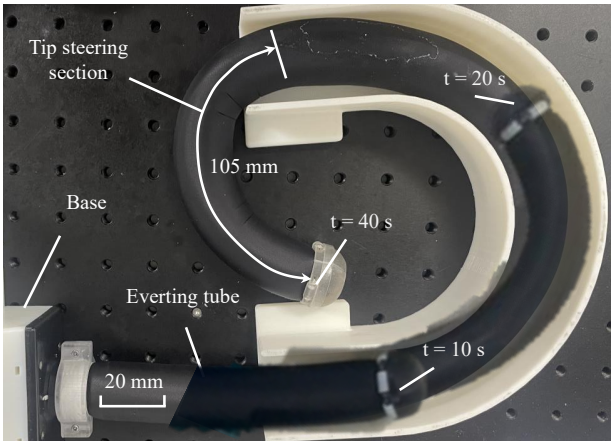

Fig. 1. Demonstration of a soft everting robot with a steerable tip, in which the body elongates via inside-out material eversion.

I. Introduction

Rigid-linked robots lack the flexibility to operate adaptively in unstructured environments. To address this limitation, soft robots, constructed from compliant materials, have been developed [1], [2]. Among them, a unique type of soft robot, the soft-growing robot, also known as vine robots, has been explored. They feature a tubular structure that everts at the tip by unfolding stored material through internal pressurisation [3]. This mode of growth allows vine robots to advance without sliding against their surroundings. Over the past decade, vine robots have demonstrated significant potentials in various areas, such as outdoor exploration [4], [5], and medical applications [6], [7].

Controlling the path of a soft everting robot is essential for its navigation, with steering being one of the biggest challenges. Typically, steering in these robots is achieved through various types of actuators integrated into the robot's outer layer, such as tendons [8] and pneumatic actuators [9].

Tendon-based steering relies on flexible, high–tensile strength cables embedded along the length of the soft robot, extending from the base to the tip [5]. These tendons are typically actuated by motors located at the robot's base. During operation, motor-driven tendon retraction generates tension that bends the body of the soft-everting robot toward the desired direction. The use of tendons offers high flexibility and compatibility with soft robotic structures. However, tendon-driven actuation suffers from friction losses. Moreover, incorporating tendon-driven mechanisms introduces manufacturing complexity, often requiring precise alignment to ensure reliable performance [10].

Pouch motors are a type of pneumatic actuator composed of sealed, flexible pouches. When pressurised, these pouches inflate and shorten along their length, causing the soft robot to bend in a desired direction. Multiple sets of pouch motors are often serially connected to achieve continuous steering and enhanced flexibility [3]. Similarly, contractive artificial muscles can reversibly shorten under internal pressurisation [11], and their contraction can induce bending in growing robots [12], [13]. One of the key advantages of pneumatic actuators lies in their lightweight design, as they contribute minimally to the overall structural mass. They can be fabricated by partially heat-sealing or bonding airtight, flexible plastic films or fabrics. However, pneumatic actuators generally exhibit a limited maximum contraction ratio of about 0.3 [9], which constrains the achievable bending radius. Moreover, their steering performance depends on the predefined arrangement of actuators, making navigation in tight or unstructured environments challenging.

Another steering approach for growing robots is the steerable tip, which refers to actuators positioned at the growing tip of robots. This mechanism enables the tip to control the overall steering direction of the entire vine robot. The

This work is supported by the Engineering and Physical Sciences Research Council, Grant EP/X033546/1 and EP/X52556X/1 (Imperial UKRI IAA) and partially supported by the InnoHK initiative of the Innovation and Technology Commission of the Hong Kong Special Administrative Region Government, Multi-Scale Medical Robotics Centre, The Chinese University of Hong Kong.

Yi Lu, Korn Borvorntanajanya, Jialei Shi, and Ferdinando Rodriguez y Baena are with Hamlyn Centre for Robotic Surgery, Department of Mechanical Engineering, Imperial College London. (e-mail: j.shi@imperial.ac.uk).

actuation of the steerable tip can be realised through various methods, including tendon-driven, magnetically driven, and pneumatically driven systems. Tendon-driven tip actuators have been demonstrated in [14], [15] to achieve planar steering. Pneumatic soft actuators, configured as two-segment [4] or one-segment [16] designs, have been developed to enable 3D steering of growing robots. In [17], a magnet was attached to the tip of a growing robot to achieve steering in confined spaces, although this approach requires an externally generated magnetic field. Furthermore, a steering method based on magnetic valves was introduced in [18], allowing selective actuation of pneumatic pouches for steering control. Localised tip steering offers a compact design and enables high-curvature steering. Steerable-tip designs allow adaptive navigation in unstructured environments.

The performance of localised tip steering is influenced by various factors, including the design of steering actuators and the selection of growth materials. However, limited studies have examined how different design parameters affect steering performance. To address this gap, this paper contributes to a comprehensive investigation into the steering performance of a soft-everting robot equipped with a pneumatically steerable tip (see Fig. 1), considering various key design parameters. Our approach integrates both finite element modelling (FEM) and experimental characterisation. Specifically, the FEM is employed to analyse the effects of manipulator geometry and material properties on steering behaviour. Experimental studies are then conducted to validate the FEM model and to evaluate steering performance using everting materials with different properties, such as thickness and stretchability.

The rest of this paper is organised as follows: Section II describes the development of the FEM. Section III validates the FEM and analyses the impact of key design parameters on steering performance, such as manipulator length and material properties. Complementary experimental investigations on fabric thickness and stretchability are presented in Section IV. Finally, the discussion and conclusions are provided in Sections V and VI, respectively.

II. Finite Element Model of the Tip Steering Mechanism

A. Overview of the Tip Steering Mechanism

The design of a tip steering mechanism (≈ 45 g) for a soft-everting robotic colonoscope is presented in [16], [19]. The mechanism consists of a pneumatic soft manipulator and an interlock cap, as illustrated in Fig. 2(a), while the steering principle is shown in Fig. 2(b). The soft manipulator is fabricated from silicone and features nine actuation chambers arranged around a central lumen through which the everting material passes. The chambers are internally connected in three groups of three [20]. To maintain the manipulator securely at the robot's tip, an interlock cap is integrated into the design. The everting material, made of Silnylon, is stretchable along the growth direction, thereby reducing the required internal pressure for eversion [12].

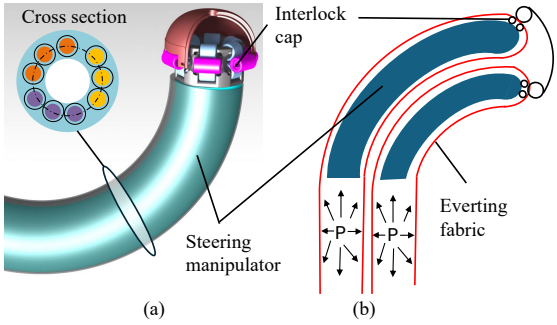

Fig. 2. (a) Details of the tip steering mechanism and its (b) schematic illustration.

The tip steering mechanism undergoes large deformations and involves highly non-linear materials, making FEA a well-suited approach for investigating its steering performance under varying design parameters, such as manipulator geometry and material properties. Please note that the maximum steering pressure is capped at 300 kPa in this work, constrained by the real robotic system [16].

B. Modelling of the Everting Fabric

The everting fabric has a thickness of 0.05 mm, a grid length of 4 mm, and a diameter of 18 mm. The developed model is shown in Fig. 3(a). The fabric is a non-homogeneous material, consisting of a reinforcement grid embedded within a base fabric of standard nylon weave. For modelling purposes, the grid pattern is treated as homogeneous nylon, while the background weave is modelled as a composite material. The material parameters for both components are summarised in Table I.

The growth pressure is applied to the inner surface of the fabric. This study investigates the quasi-static scenarios, therefore, the growth pressure increments follows a smoothstep function, resulting in a smooth transition of a variable between two desired magnitudes. The smoothstep is as follows:

$$\text{Smoothstep}(x,a,b) = 3t^2 - 2t^3, \quad t = \frac{x-a}{b-a} \tag{1}$$

where x is the input variable to be interpolated, which is considered the growth pressure in this case. a and b refer to the initial and final values of x, and t is the normalised value of x in the range of $[a,b]$, scaled to $[t_1,t_2]$. At $t_1 = 0$ s, the magnitude of the growth pressure is 0, and at $t_2 = 0.5$ s, the magnitude of the growth pressure reaches its maximum, which is kept at 15 kPa for further comparison.

The mesh refinement of the fabric model is shown in Fig. 3(b). The whole structure is meshed using explicit

TABLE I

Elastic Behaviour of Different Sections of the Fabric [21] [22]

Material Section	Young's Modulus (MPa)	Poisson's Ratio
Reinforcement Grid	3000	0.3
Background Weave	30	0.3

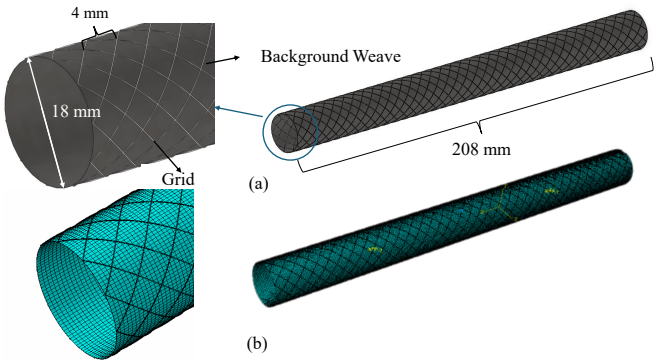

Fig. 3. (a) Model of the fabric and its (b) mesh.

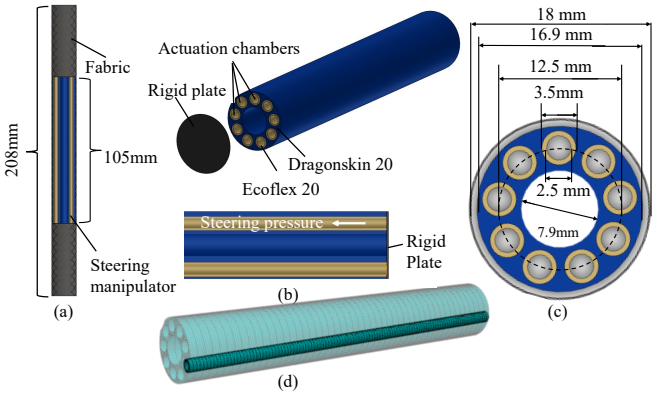

Fig. 4. (a) The steering manipulator inside of the fabric. (b) Details of the manipulator and its (c) cross section. (d) Mesh model of the manipulator.

C3D8R elements, which are 8-node linear bricks with reduced integration and hourglass control. The grid section and the background weave section have different global seeding sizes, set to 0.2 and 0.5, respectively. The overall number of elements in the fabric model is 155316.

C. Modelling of the Steering Manipulator

The steering manipulator is inside of the fabric (see Fig. 4(a)), with its dimensions illustrated in Figs. 4(b)-(c). To simplify the simulation, the interlock cap is omitted from the model, while the fabric length is set to 208 mm, sufficient to cover the entire manipulator during bending. The manipulator consists of two nonlinear materials, which are set as Dragon Skin 20 and Ecoflex 20 for this prototype. Two rigid plates are tied to the two ends of the manipulator, which seals the pressure inside the manipulator. These plates are set as rigid bodies, with their reference point at the centre, preventing any deformation of the plate in the simulation.

Dragon Skin 20 and Ecoflex 20 are hyper-elastic. Considering the available nonlinear model in Abaqus, these materials are defined by using the second-order Yeoh model. This model fits the stress-strain behaviour of a material according to the (2) [23]. Two model coefficients C_1, C_2 are required, with their values reported in Table II.

$$\sigma_{\text{uniax}} = 2\left(\lambda^2 - \frac{1}{\lambda}\right)\sum_{i=1}^{2} i \cdot C_i (I_1 - 3)^{i-1} \tag{2}$$

where λ denotes the longitudinal stretch, and σ_{uniax} is the corresponding stress. Steering pressure is applied inside of the actuation chambers, exerting force on the rigid plate, as shown in Fig. 4(b). Smoothstep interpolation is applied to the steering pressure. At t_1 = 0 s, the magnitude of the steering pressure is 0, and at t_2 = 1 s, the magnitude of the steering pressure reaches the maximum, which is kept as 300 kPa.

The mesh refinement of the manipulator uses C3D8R element from the explicit library as before. The meshing of each component is carried out separately. The meshing of the Dragon Skin 20 component, shown in Fig. 4(d), has an approximate global size of 0.3, as it has a complex geometry that needs more elements to define. Local seeding is applied to the length of the component, with the number of elements controlled to be 50. The Ecoflex 20 component, has a global size of 0.5. To mesh the component according to its cylindrical geometry, local seeding defines 2 elements along the radial direction, 36 elements along the tangential direction, and 50 elements along the longitudinal direction. Rigid plate has an approximate global size of 0.6. The overall meshing of the manipulator has elements of 130872.

The fabric and steering manipulator are assembled by positioning the manipulator inside of the fabric. General contact is defined globally across the model. The contact properties are specified such that the tangential behaviour is frictionless, while the normal behaviour employs a 'Hard' contact formulation with default constraint enforcement, allowing separation after contact.

III. Finite Element Analysis of the Steering Performances

A. Validation of the FEM Model

The developed model of the soft everting robot needs to be validated before it can be used for further design analysis. The maximum steering pressure of the prototype is varied from 50 kPa to 300 kPa in steps of 50 kPa.

To deduce the steering angle of the simulations, three coordinates are randomly selected at each end of the fabric, with six coordinates selected in total, represented as points A_1, A_2, and A_3 for the first surface, and B_1, B_2, and B_3 as the second surface. Three points are sufficient to define a surface, with respect to its normal vectors:

$$\vec{n}_A = (\vec{A}_2 - \vec{A}_1) \times (\vec{A}_3 - \vec{A}_1), \tag{3}$$

$$\vec{n}_B = (\vec{B}_2 - \vec{B}_1) \times (\vec{B}_3 - \vec{B}_1). \tag{4}$$

TABLE II
Yeoh Model Coefficients of Ecoflex 20, Ecoflex 50, Dragonskin 10, Dragonskin 20 and Dragonskin 30 [23]

Material	C_1	C_2
Ecoflex 20	0.0077	0.0002
Ecoflex 50	0.011771	0.000159
Dragonskin 10	0.039695	0.000627
Dragonskin 20	0.1062	0.0018
Dragonskin 30	0.1313	0.002546

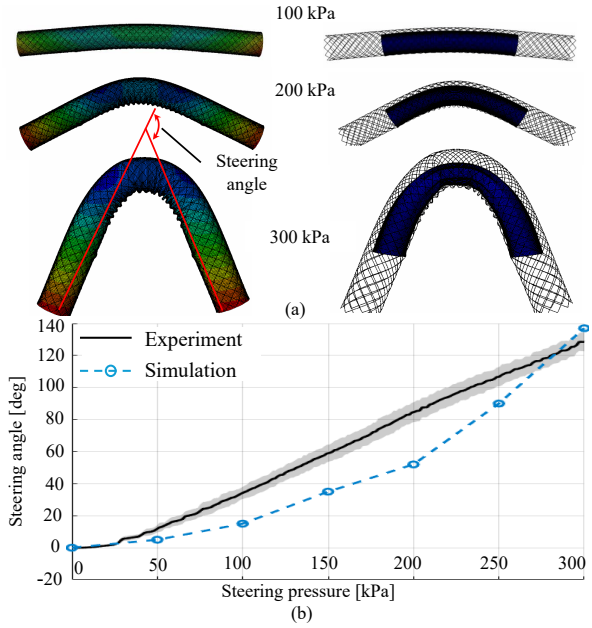

Fig. 5. (a) Simulation results of the steering performances of the prototype with steering pressure at 15 kPa growth pressure. (b) Comparison of steering angles between the FEA and experiments at a growth pressure of 15 kPa. The experimental setup is reported in Section IV-A. As described in Section II-B, Fabric 3 (see Table III) is simulated.

The angle θ between the normal vectors is taken as the steering angle (see Fig. 5(a)):

$$\theta = \cos^{-1}\left(\frac{\vec{n}_A \cdot \vec{n}_B}{\|\vec{n}_A\| \cdot \|\vec{n}_B\|}\right), \tag{5}$$

Figs. 5(a) and (b) show snapshots of the simulations alongside the steering angles obtained from both simulations and experiments. Simulation errors are about $20^\circ \sim 30^\circ$ especially when the steering pressure is between 150 kPa and 200 kPa. The maximum steering angle from the simulation and the experiment is 134° and 128°. The simulation error decreases at the maximum steering pressure, which can be attributed to the FEM model representing a quasi-static problem, where higher accuracy is expected at the final stage of deformation. Consequently, the maximum steering angle is used for the design analysis in the subsequent sections.

B. FEM-based Design Analysis

Based on the validated FEM model, various design parameters can be investigated, such as material properties and manipulator dimensions. In all simulations, the grid width is 4 mm, and the fabric thickness is 0.05 mm.

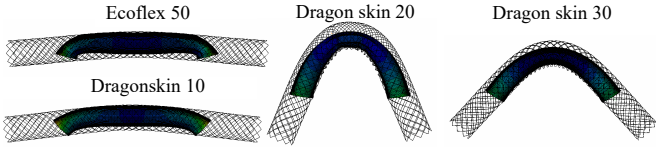

Fig. 6. Steering performance of the soft everting robot with different manipulator material at 15 kPa growth pressure.

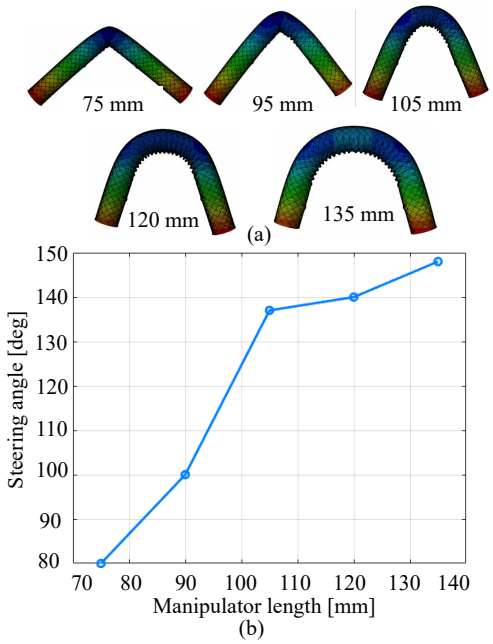

Fig. 7. (a) Simulation results and (b) steering angle of the soft everting robot with varying manipulator length at 15 kPa growth pressure.

1) Steering Angle and Manipulator Material: Four silicone materials, Ecoflex 50 and Dragon Skin 10, 20, and 30, used for the steering manipulator are investigated, with their material parameters listed in Table II. Please note that the chamber material remains as Ecoflex 20 (see Fig. 4). In the simulations, a growth pressure of 15 kPa is applied, and the maximum steering pressure is limited to 300 kPa.

The steering performance with different manipulator materials is reported in Fig. 6. It is observed that for manipulators using Ecoflex 50 and Dragon Skin 10, the manipulator cannot bend the fabric even at a high steering pressure, and as for manipulators made of Dragon Skin 30 instead of Dragon Skin 20, the result retains a constant curvature pattern, but shows a reduction in the maximum steering angle from 134 degrees to 87 degrees.

2) Steering Angle and Manipulator Length: Manipulator length is another key design parameter influencing steering performance. In the simulations, this length is varied from 75 mm to 135 mm in 15 mm increments. The steering pressure is set as 300 kPa.

The resulting steering performance and corresponding angles are shown in Fig. 7. As the manipulator decreases from 105 mm to 75 mm, the steering angle reduces from 134 degrees to 90 degrees. As the manipulator increases from 105 mm to 135 mm, there is a slight increase in the steering angle from 134 degrees to 148 degrees. A longer manipulator is able to retain the uniform curvature pattern along the length, but it can be seen that a larger steering radius is required to steer a longer manipulator, with the radius of steering changing from 22 mm to 42 mm.

3) Steering Angle and Fabric Strength: Fabric material properties can also significantly influence steering performance. In the finite element analysis, different fabric mate-

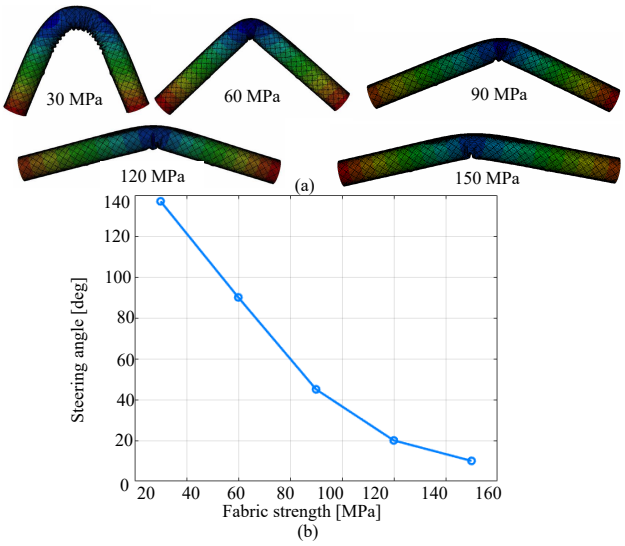

Fig. 8. (a) Steering performance of the robot with varying fabric strength at 15 kPa growth pressure. (b) Steering angle versus the fabric strength.

rials are represented by variations in fabric strength. Specifically, the Young's modulus of the fabric's background weave is varied from 30 MPa to 150 MPa in 30 MPa increments to evaluate its impact on steering behaviour. The steering pressure is set as 300 kPa.

The steering performance and the related steering angles are shown in Fig. 8. The result shows that lower fabric strength leads to a relatively higher steering angle, as the angle decreases from 134 degrees to 5 degrees when the fabric strength increases from 30 MPa to 150 MPa. It should be noted, however, that fabrics with lower strength may be unable to withstand the required growth pressure, potentially leading to excessive distortion.

The FEM model is a valuable tool for exploring various design parameters, particularly the design of the soft manipulator prior to robot fabrication. However, the model relies on certain assumptions, and fabric properties cannot be fully captured by changes in material strength alone. As an anisotropic material, fabric exhibits complex mechanical properties—such as elasticity, stretchability, and friction—that directly affect steering performance. A more comprehensive investigation of the design parameters of everting materials is conducted through experimental characterisation, as described in Section IV.

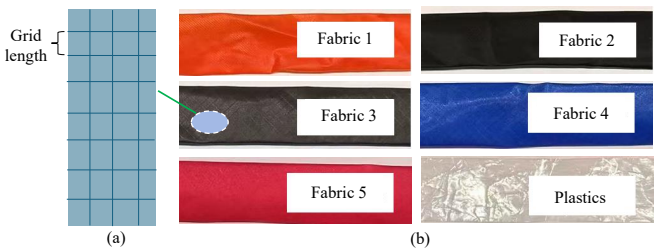

Fig. 9. (a) Illustration of grid length and (b) six everting materials.

TABLE III
PARAMETERS OF SIX EVERTING MATERIALS

Fabrics	Thickness (mm)	Grid length (mm)	Supplier
Fabric 1	0.03	1	Ripstop by the Roll
Fabric 2	0.05	1	Ripstop by the Roll
Fabric 3	0.05	4	Ripstop by the Roll
Fabric 4	0.06	3	Seattle Fabrics
Fabric 5	0.09	3	UK Fabrics Online
Plastic	0.05	N/A	Xin Chengxiang Package

IV. Experimental Characterisation of Everting Materials and the Steering Angle

Ripstop nylon fabrics and plastics are commonly used in soft-everting robots, with fabrics offering high tear resistance and durability. For this study, five commercially available ripstop nylon fabrics with thicknesses suitable for soft-growing robots were selected for comparison. In addition, one plastic material, commonly used in other soft robots, was included for comparative analysis. The six materials are shown in Fig. 9, and their parameters, including thickness and grid pattern length, are summarised in Table III.

A. Experimental Setup

The growth pressure and the steering pressure are regulated by one SMC ITV1050 and three SMC ITV2010 pressure regulators, respectively. A micro-controller (Teensy 4.1) communicates with two DAC converters (Adafruit MCP4728) via I2C to set pressure control signals. Matlab and the Teensy board communicates via the serial port. The steering angle or displacement are measured by an electromagnetic (EM) tracking device (Aurora, NDI).

B. Experiment 1 - Characterisation of the Stretchability of Different Everting Materials

1) Experimental Protocol: The contraction behaviour is observed only in fabrics with a 45° grid orientation along the axial direction. Six different materials were tested under growth pressures of 5, 10, 15, and 20 kPa. An EM tracker was attached to the tip of the tube to measure displacement

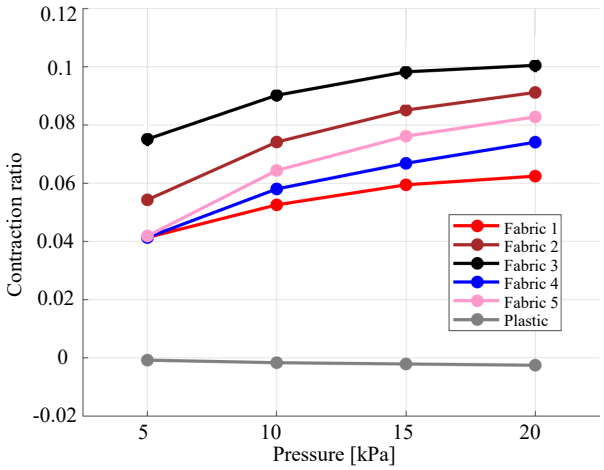

Fig. 10. Results for Experiment 1: Contraction ratio of six materials under different growth pressure.

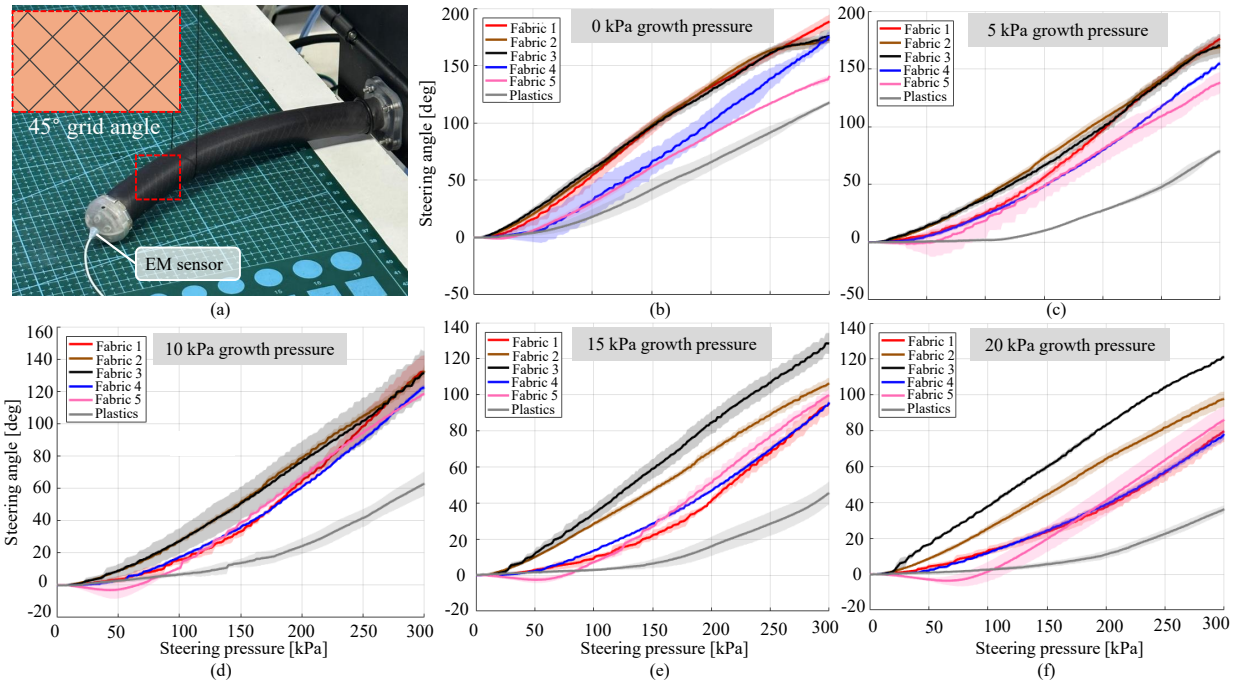

Fig. 11. Results for Experiment 2: Characterisation of the steering angle using different materials. (a) Steering angle measurement. For fabrics, the grid angle is 45° to the growth direction. The steering angle at the growth pressure of (b) 0 kPa, (c) 5 kPa, (d) 10 kPa, (e) 15 kPa, and (f) 20 kPa.

variations during pressurisation, with each test performed in three repeated trials to ensure repeatability.

2) Results: The contraction ratios of the six materials are shown in Fig. 10. For the fabric samples, the contraction ratios range from 0.04 to 0.10. Among them, Fabric 3 consistently demonstrates the highest contraction ratio, reaching 0.10, followed by Fabric 2 (0.09), Fabric 5 (0.07), Fabric 4 (0.07), and Fabric 1 (0.06). In contrast, the plastic sample exhibits a negative contraction ratio, indicating that it expands rather than contracts under internal pressure.

C. Experiment 2 - Steering Angle from Various Everting Materials Aligned to a 45-Degree Grid

1) Experimental Protocol: The growth pressure was varied between 0 and 20 kPa, while the steering pressure was linearly increased from 0 to 300 kPa over 20 s. The Dragon Skin 20 manipulator was selected for this experiment based on the results in Section III-B.1. During each test, one set of actuation chambers of the manipulator was pressurised. Six different fabric materials were evaluated under four growth pressure conditions (0, 5, 10, 15, and 20 kPa). In each test, three repeated trials were conducted to ensure repeatability. The steering angle of the manipulator was recorded using an EM tracker (see Fig. 11(a)).

2) Results: The steering angle with steering pressure under different growth pressure, with a grid configuration at a 45-degree angle to the growth direction, is reported in Fig. 11. At a growth pressure of 0 kPa, the steering angles of Fabric 2, Fabric 3, and Fabric 4 exhibit similar values, reaching approximately 175 degrees at a steering pressure of 300 kPa. Fabric 1 shows a slightly higher angle of 190 degrees, while Fabric 5 shows a smaller angle of 140 degrees.

As the growth pressure increases, the steering angle decreases. At an intermediate growth pressure of 10 kPa, among the ripstop nylon materials, Fabric 1 undergoes the largest decrease in steering angle from 190 degrees to 130 degrees. Fabric 3 also exhibits a large reduction from 175 degrees to 120 degrees. By contrast, Fabric 2 and 3 have a smaller reduction from 175 degrees to 135 degrees. Fabric 5 has the smallest reduction in angle, from 140 degrees to 120 degrees. At a high growth pressure of 20 kPa, Fabric 3 achieves the largest steering angle, reaching 120 degrees at 300 kPa steering pressure. This is followed by Fabric 2, Fabric 5, Fabric 1, and Fabric 4, with steering angles of 95 degrees, 82 degrees, 80 degrees, and 79 degrees, respectively.

As for the homogenous plastic material, it has a steering angle of 120 degrees at 0 kPa growth pressure. As the plastic is pressurised, the steering angle dramatically decreases to 80 degrees at 5 kPa growth pressure, and continues to decrease to only 38 degrees at 20 kPa growth pressure. This has a significant difference from the fabrics, indicating that the steering performance of plastic is substantially poorer than ripstop nylon fabrics when the reinforcement grid is oriented at 45 degrees to the growth direction.

D. Experiment 3 - Steering Angle from Various Everting Materials Aligned to a 0-Degree Grid

1) Experimental Protocol: The steering pressure linearly increased from 0 kPa to 300 kPa in 20 s. Three trials are conducted in each test. Six different fabric materials with four different growth pressures (0, 5, 10, 15, and 20 kPa) were explored. An EM tracker measured the steering angle (see Fig. 12(a)).

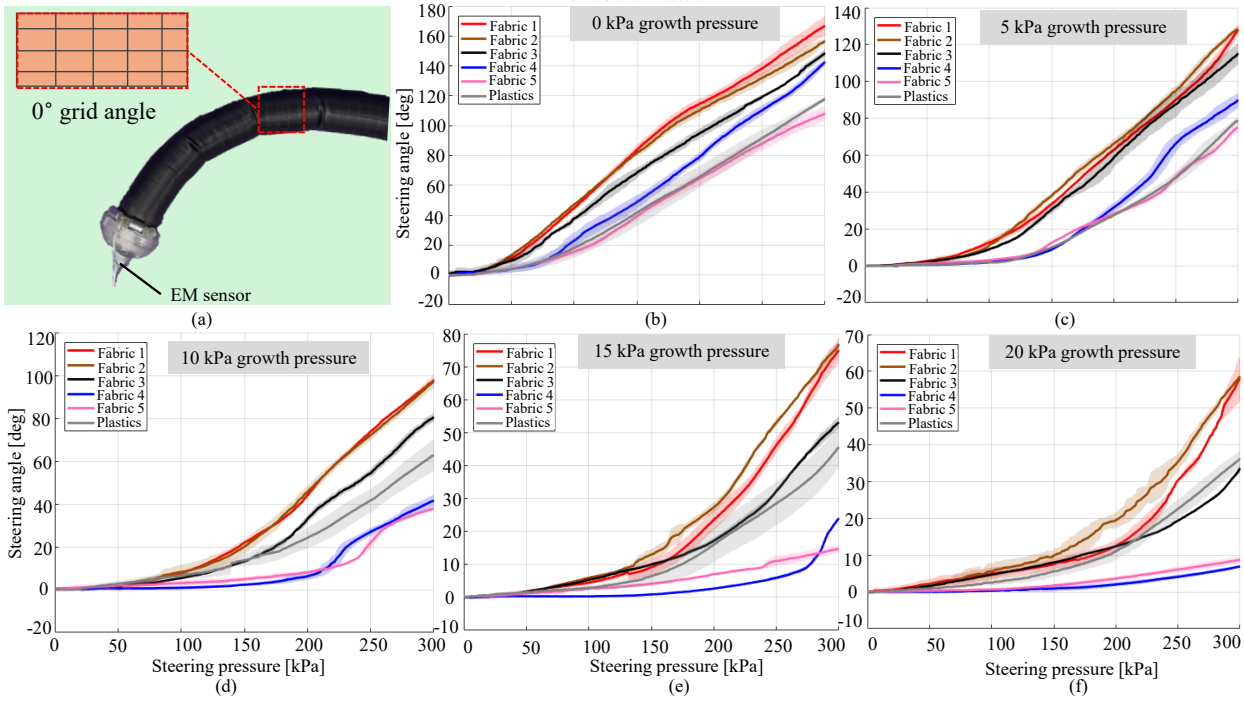

Fig. 12. Results for Experiment 3: Characterisation of the steering angle using different materials. (a) Steering angle measurement. For fabrics, the grid angle is 0° to the growth direction. The steering angle at the growth pressure of (b) 0 kPa, (c) 5 kPa, (d) 10 kPa, (e) 15 kPa, and (f) 20 kPa.

2) Results: Steering angles under different growth pressure, with a grid configuration of 0-degree angle to the growth direction, are reported in Fig. 12. At a growth pressure of 0 kPa, the steering angle is similar to the 45-degree configuration samples. Thinner fabric, such as Fabric 1, exhibits a relatively larger angle of 170 degrees, while thicker fabric, such as Fabric 5, exhibits a smaller angle of only 104 degrees. As the growth pressure increases, the steering angle drops dramatically. At an intermediate growth pressure of 10 kPa, Fabric 1 and Fabric 2 drop from 170 degrees to 100 degrees, Fabric 3 drops from 140 degrees to 80 degrees, and Fabric 4 and 5 drop to only 40 degrees. This shows a huge contrast when compared with samples of different grid configurations.

This trend also applies to higher growth pressure conditions. At a growth pressure of 20 kPa, angles from Fabric 1 and 2 drop from 100 degrees to 60 degrees, angle from Fabric 3 drops from 80 degrees to 30 degrees, and angles from Fabric 4 and 5 drop to 10 degrees. At high growth pressure, it can be seen that the steering angle doesn't increase proportionally with the increase in steering pressure. At low steering pressure, there is barely any increase in the steering angle, but when the steering pressure reaches 200 kPa, the rate of change of angle increases sharply. The steering performance of soft everting robots fabricated with plastics is found to be similar to those using thinner nylon fabrics with a 0-degree grid configuration.

V. Discussions

The FEM aligns with the experimental results under the maximum steering pressure. However, there are non-negligible errors when the pressure is low (see Fig. 5(b)). For finite element analysis, considering the computational limitation, mass scaling was enabled to reduce simulation time. While mass scaling significantly improves computational efficiency, it sacrifices certain accuracy, potentially causing errors. Findings from the FEM model confirm that key parameters, such as manipulator length, material, and fabric characteristics, significantly influence the steering performance. Section III-B.1 examines the effect of manipulator material. The results show that samples made from Dragon Skin 10 and Ecoflex 50 fail to bend the fabric under high growth pressures, as these softer manipulators tend to deform internally within the fabric. In contrast, Dragon Skin 30 produces smaller steering angles under equivalent pressurisation, whereas Dragon Skin 20 achieves the largest steering angles, making it the preferred material choice. Section III-B.2 explores the influence of manipulator length on steering behaviour. The results indicate that shorter manipulators generate smaller steering angles, while longer manipulators suffer reduced manoeuvrability, showing only a marginal increase in steering angle but a significantly larger steering radius. A larger steering radius is undesirable for navigating tight bends, such as those found in the human colon [6].

Fabric properties influence steering performance in multiple ways. Section III-B.3 investigates the effect of fabric strength, showing that lower fabric strength results in improved steering performance. Section IV further examines other fabric characteristics, including thickness and grid configuration, through experimental characterisation. Overall, an increase in growth pressure leads to a reduction in steering angle. At low growth pressures, fabric thickness is the

TABLE IV

SUMMARY OF FINDINGS ON KEY DESIGN PARAMETERS

Design factors	Recommendations
Types of tube materials	Silnylon (low friction, high durability)
Types of coating	Double-sided silicone coating (low frictions)
Silnylon thickness	$<$ approx. 0.05 mm, i.e., $<$ 1.1 oz
Axial stretchability	At least approx. 0.1, i.e., grid size $>$ 3-4 mm
Manipulator materials	100% modulus $>$ 250 kPa (Dragon Skin Series)
Manipulator length	At least $<$ approx. 100 mm

dominant factor, i.e., thicker fabrics produce smaller steering angles, as they introduce greater resistance and require more force to deform. At high growth pressures, the grid configuration becomes more significant: fabrics with a 45-degree grid orientation relative to the growth direction achieve substantially larger steering angles compared to those with a 0-degree orientation. We attribute this to bias-cut mechanics: at 45 degrees, the grid deforms mainly by in-plane shear, reducing the wall's effective axial stiffness and enabling greater bend. By contrast, a 0-degree orientation aligns fibres with the axis, increasing axial tension as pressure rises and thereby suppressing curvature. As such, fabrics with a higher contraction ratio not only require lower growth pressure [24], which also result in better steering performances under a high growth pressure (see Fig. 10 and Fig. 11(f)).

In summary, Table IV highlights key design recommendations across the investigated parameters. While the findings are derived from the 18 mm-diameter robot reported in [16], they potentially offer transferable insights for the design of steering mechanisms in larger-scale everting robots, such as Roboa [4]. Nevertheless, several limitations remain. The FEM in this work is intended as a comparative design tool rather than a precise model, and the simplified FEM and focuses on a quasi-static case: the fabric's background weave is treated as a homogeneous material rather than explicitly modelled as a woven structure. In addition, the interlock tip is not included in the FEM. These simplifications were introduced to enhance computational efficiency. In future work, the model's accuracy could be improved by employing a more detailed FEM implemented on high-performance computing platforms. In addition, analytical methods could also be explored to ease computation complexity [25].

VI. CONCLUSIONS

This paper presents a comprehensive investigation into the tip steering performance of soft everting robots, integrating finite element simulations and experimental characterisation. The developed FEM predicts the quasi-static steering behaviour of everting robots, highlighting the impact of key parameters such as manipulator length, material properties, and fabric strength. Experimental characterisation complements the simulations by exploring other fabric properties, including thickness and grid patterns. Together, these findings offer practical insights and design guidelines for optimising pneumatic steering tips in soft everting robots (see Table IV).

REFERENCES

[1] M. Yip *et al.*, "Artificial intelligence meets medical robotics," *Science*, vol. 381, no. 6654, pp. 141–146, 2023.

[2] J. Shi, A. Shariati, S.-A. Abad, Y. Liu, J. S. Dai, and H. A. Wurdemann, "Stiffness modelling and analysis of soft fluidic-driven robots using Lie theory," *Int. J. Rob. Res.*, vol. 43, no. 3, pp. 354–384, 2024.

[3] M. M. Coad *et al.*, "Vine robots," *IEEE Robot. Autom. Mag.*, vol. 27, no. 3, pp. 120–132, 2020.

[4] P. A. der Maur *et al.*, "Roboa: Construction and evaluation of a steerable vine robot for search and rescue applications," in *Proc. IEEE Int. Conf. Soft Robot.*, 2021, pp. 15–20.

[5] N. D. Naclerio *et al.*, "Controlling subterranean forces enables a fast, steerable, burrowing soft robot," *Sci. Rob.*, vol. 6, no. 55, p. eabe2922, 2021.

[6] K. Borvorntanajanya, S. Treratanakulchai, F. R. y. Rodriguez, and E. Franco, "Model-based tracking control of a soft growing robot for colonoscopy," *IEEE Trans. Med. Robot. Bionics.*, vol. 6, no. 4, pp. 1354–1362, 2024.

[7] A. Giri, C. Girerd, J. Cervera-Torralba, M. T. Tolley, and T. K. Morimoto, "Inchigrab: An inchworm-inspired guided retraction and bending device for vine robots during colonoscopy," *IEEE/ASME Trans. Mechatronics*, vol. 30, no. 6, pp. 6870–6881, 2025.

[8] L. H. Blumenschein *et al.*, "Geometric solutions for general actuator routing on inflated-beam soft growing robots," *IEEE Trans. Robot.*, vol. 38, no. 3, pp. 1820–1840, 2022.

[9] A. M. Kübler *et al.*, "A comparison of pneumatic actuators for soft growing vine robots," *Soft Rob.*, vol. 11, no. 5, pp. 857–868, 2024.

[10] S. Al Harthy *et al.*, "Tip-growing robots: Design, theory, application," *IEEE Trans. Robot.*, vol. 41, pp. 5511–5532, 2025.

[11] S. M. Mirvakili and I. W. Hunter, "Artificial muscles: Mechanisms, applications, and challenges," *Adv. Mater.*, vol. 30, no. 6, p. 1704407, 2018.

[12] N. D. Naclerio and E. W. Hawkes, "Simple, low-hysteresis, foldable, fabric pneumatic artificial muscle," *IEEE Trans. Robot. Autom.*, vol. 5, no. 2, pp. 3406–3413, 2020.

[13] N. G. Kim *et al.*, "A soft growing robotic endoscope for painless and strain-free insertion," *Soft Rob.*, pp. 1–14, 2025.

[14] T. Takahashi *et al.*, "Eversion robotic mechanism with hydraulic skeleton to realize steering function," *IEEE Trans. Robot. Autom.*, vol. 6, no. 3, pp. 5413–5420, 2021.

[15] D.-G. Lee, N. G. Kim, and J.-H. Ryu, "High-curvature consecutive tip steering of a soft growing robot for improved target reachability," in *Proc. IEEE/RSJ Int. Conf. Intell. Robots Syst.*, 2023, pp. 6477–6483.

[16] J. Shi, K. Borvorntanajanya, K. Chen, E. Franco, and F. R. y. Baena, "Design, control, and evaluation of a novel soft everting robot for colonoscopy," *IEEE Trans. Robot.*, vol. 41, pp. 4843–4859, 2025.

[17] N. G. Kim *et al.*, "External steering of vine robots via magnetic actuation," *Soft Rob.*, vol. 12, no. 2, pp. 159–170, 2025.

[18] A. M. Kübler *et al.*, "A multi-segment, soft growing robot with selective steering," in *Proc. IEEE Int. Conf. Soft Robot.*, 2023, pp. 1–7.

[19] K. Borvorntanajanya *et al.*, "A pneumatic force sensor for enhanced force feedback in robotic colonoscopy," *IEEE Trans. Med. Robot. Bionics.*, vol. 7, no. 4, pp. 1377–1388, 2025.

[20] J. Shi *et al.*, "Miniaturised soft manipulators with reinforced actuation chambers on the sub-centimetre scale," in *Proc. IEEE Int. Conf. Soft Robot.*, 2024, pp. 157–164.

[21] A. Djoumessi, N. Tagne, T. Stanislas, F. Ngapgue, and N. ebénézer, "Optimization of the Young's modulus of woven composite material made by raphia vinifiera fiber/epoxy," *Int. J. Simul. Multidiscip. Des. Optim.*, vol. 13, 10 2022.

[22] W. D. Callister and D. G. Rethwisch, *Materials Science and Engineering: An Introduction*, 9th ed. John Wiley & Sons, 2013.

[23] L. Marechal *et al.*, "Toward a common framework and database of materials for soft robotics," *Soft Rob.*, vol. 8, no. 3, pp. 284–297, 2021.

[24] D. A. Haggerty, N. D. Naclerio, and E. W. Hawkes, "Characterizing environmental interactions for soft growing robots," in *Proc. IEEE/RSJ Int. Conf. Intell. Robots Syst.*, 2019, pp. 3335–3342.

[25] J. Shi *et al.*, "A static modelling and evaluation framework for soft continuum robots with reinforced chambers," *IEEE Trans. Robot.*, vol. 41, pp. 6419–6439, 2025.